Journal of Intelligent & Robotic Systems (2020) 100:389–400
https://doi.org/10.1007/s10846-020-01200-5

Model-based Control with Interaction Predicting for Human-coupled Lower Exoskeleton Systems

Guangkui Song[1] · Rui Huang[1] · Jing Qiu[1] · Hong Cheng[1] · Shuai Fan[2]

Received: 3 July 2019 / Accepted: 6 April 2020 / Published online: 23 April 2020

Abstract

Sensitivity Amplification Control (SAC) algorithm was first proposed in the augmentation application of the Berkeley Lower Extremity Exoskeleton (BLEEX). Since the SAC algorithm can greatly reduce the complexity of exoskeleton system, it is widely used in human augmentation applications. Nevertheless, the performance of the SAC algorithm depends on the accuracy of dynamic model parameters. In this paper, we propose a novel Model-based control with Interaction Predicting (MIP) strategy to lower dependency on the accurate dynamic model of the exoskeleton. The MIP consists of an interaction predictor and a model-based controller. The interaction predictor can predict motion trajectories of the pilot and substitute for the pilot to drive the exoskeleton through an impedance model. In proposed strategy, the model-based controller not only amplify the forces initiated by the interaction predictor, but more importantly the forces imposed by the pilot to correct the errors between the predictive motion trajectory and the intended motion trajectory of the pilot. Illustrative simulations and experimental results are presented to demonstrate the efficiency of the proposed strategy. Additionally, the comparisons with traditional model-based control algorithm are also presented to demonstrate the efficiency and superiority of the proposed control strategy for lowering dependency on dynamic models.

Keywords Model-based control with interaction predicting · Sensitivity amplification control · Inaccurate dynamic model · Physical human-robot interaction · Strength augmentation · Lower exoskeleton

1 Introduction

Lower extremity exoskeletons are wearable robotic systems, they can effectively augment the performance of pilots by wearing it on the body. They integrate human intelligence and robot power, effectively avoiding the shortcoming of both. Thanks to the development of wearable technologies, lower extremity exoskeletons have been developed into nearly commercialized products and applied in real-world scenarios [7, 13, 15, 21, 24] over the last few decades. As lower extremity exoskeleton is tightly coupled with human beings, it requires an ability that it can follow the pilot's motion with minimal resistance (i.e. little interaction forces between the exoskeleton and the pilot). For human-robot interaction related applications, the sense-act-modulated-byinteractions (SAMI) architecture [1] is proposed and a development methodology [19] on human-robot interaction is proposed to support the robot standardization effort.

For different application scenarios, corresponding control algorithms are demonstrated for lower extremity exoskeletons. Among them, the Berkeley Lower Extremity EXoskeleton (BLEEX) is the famous one for field applications, in which the Sensitivity Amplification Control (SAC) algorithm can greatly simplify the complexity of exoskeleton system. So, it is widely chosen for human augmentation applications. The SAC algorithm is used as a high-level control strategy in HUman-powered Augmentation Lower EXoskeleton (HUALEX) [8], in which the introduction of Reinforcement Learning (RL) has improved the adaptability to the changing with different pilots and walking patterns. In order to better describe different motion trajectories of the pilot, Hierarchical Interactive Learning (HIL) strategy is proposed [9, 11] with an imitation learning-Dynamic

✉ Guangkui Song
sgk095@gmail.com

[1] Center for Robotics, School of Automation and Engineering, University of Electronic Science and Technology of China, Chengdu, China

[2] School of Mechanical and Electrical Engineering, University of Electronic Science and Technology of China, Chengdu, China

movement primitives (DMP). In [10], the real-time interaction term between the pilot and the exoskeleton is modeled through impedance model to achieve the proactive modeling of human motion trajectories, and the parameters of the impedance model are learned online by a RL method. In the mentioned applications, the SAC is used as a high-level control algorithm. The goal of SAC algorithm is to make the interaction forces between the exoskeleton and the pilot as small as possible without measuring any information of the pilot. However, SAC algorithm is a typical model-based control method, so accurate dynamic models are required. The performance of SAC algorithm is greatly affected by the error of dynamic model parameters. And the identification process of dynamic model is extremely complicated [5, 6] and the dynamic model is time-varying due to unexpected mechanical vibrations [16]. In other word, the performance of the SAC algorithm depends on the accuracy of dynamic model parameters.

To achieve more precise modeling of industrial robots, multi-body modelling softwares are created for replacing pen and paper. In [6, 23], the swing leg is modeled as a two-dimensional three-segment manipulator. The length of the thigh and shank links is determined by direct measurement. The mass moment parameters, inertial parameters, stiffness torques, damping and friction torques can be identified by least squares estimation. For dealing with complex dynamics, learning methods are used to approximate the dynamic model for model-based robot control, such as Local Gaussian Process Regression (LGPR) [18], RL [17]. For repetitive processes and run-based processes, Iterative Learning Control (ILC), Repetitive Control (RC), and Run-to-Run control (R2R) play an important role [4, 25]. Which can find a optimal scheme from repetitive task in the automatic operation of dynamic systems. However, in applications of coupled the human-exoskeleton system, the interaction factors can affect the control performance. Literature [22] considers that in a human-exoskeleton interaction application the interaction torque resulted from the pilot can determined by normal physical mathematical model. So Locally Weighted Regression (LWR) is used to learn physical human-exoskeleton interaction dynamics. As lower extremity exoskeleton is tightly coupled with human beings, the interaction factor and the dynamic of exoskeleton should be considered as one dynamic system.

In this paper, we propose a Model-based control with Interaction Predicting (MIP) strategy which can lower dependency on the accurate dynamic model of exoskeletons. The MIP strategy is based on model-based control and takes advantages of model-based control to greatly simplify the complexity of exoskeleton system [11]. In addition, the addition of an interaction predictor can overcome the main drawback of model-based control: requiring accurate dynamic models of the exoskeleton (includes effects of interaction factor and errors of dynamic model). The goal of the proposed strategy is to reduce the physical interaction forces between the pilot and the exoskeleton with inaccurate dynamic models of the exoskeleton. In MIP strategy, an interaction predictor can generate a proactive motion trajectory of the pilot base on gait descriptors such as historical information and substitute for the pilot to drive the exoskeleton through an impedance model. In traditional model-based algorithm (such as the SAC algorithm), the pilot drives the exoskeleton forcibly to manage inaccurate dynamic models of the exoskeleton. That is to say, the inaccurate dynamic models result bigger interaction forces. In proposed MIP, the inaccurate dynamic models are managed by the interaction predictor substituted for the pilot. The model-based controller not only amplify the forces initiated by the interaction predictor but also allow the pilot to easily correct the errors between the predictive motion trajectory and the intended motion trajectory of the pilot through amplifying the forces of the pilot. Through above methods, we can effectively lower down the dependency on accurate dynamic models of the exoskeleton, and design simulation experiments and actual wear experiments to fully verify our strategy. In the experiment, the same motion curve and dynamic model error were designed to compare MIP and SAC control strategies. The interaction force between the exoskeleton and the pilot is used to measure the superiority of the control strategy.

The main contributions of this paper can be summarized and emphasized as follows:

- We bring about a novel MIP strategy to lower dependency on the accurate dynamic model of exoskeletons.
- Specific interaction predictor is used to generate proactive motion trajectories of the pilot and substitute for the pilot to drive the exoskeleton through an impedance model. The model-based controller not only amplify the forces initiated by the interaction predictor but also help the pilot easily correct the errors.
- The comparisons on a single Degree Of Freedom (DOF) exoskeleton platform demonstrate the advantages of the MIP strategy, and the verifications on HUALEX system proves that our works are useful.

The structure of this paper is organized as follows: Section 2 addresses the design of the proposed MIP strategy. Illustrative simulations and corresponding experimental results on a single DOF exoskeleton and HUALEX system are shown in Section 3, and we detail the comparisons with traditional model-based control algorithms. The end is coming with conclusions and future works in Section 4.

2 Model-based Control with Interaction Predicting Strategy

According to the study of biomechanics and dynamics, several distinct phases can be abstracted from normal walking gait [26]. In this paper, we divide normal walking gait into stand phases and swing phases. The main function of the stand phase is to transfer loads to the ground; unload movements are performed in the swing phase and the swing phase has a wide range of motions with high bandwidth refer to the stand phase. The issue of following ability is sharper in the swing phase. Therefore, the proposed MIP strategy is mainly used for the swing phase. An exoskeleton interacting with a pilot during walking motion represents as Fig. 1. The encoder integrated in joints can read the angular disturbance resulted from the pilot. Accoding to the angular disturbance, the MIP strategy can provide τ to drive the exoskeleton. The inclinometer set in the backpack used to provide the gait descriptors for the MIP strategy.

The advantage of the MIP strategy is that it can lower dependency on accurate dynamic models of the exoskeleton as Fig. 2. The strategy is mainly composed of two parts: 1) an interaction predictor; 2) a model-based controller. We use the interaction predictor to generate proactive motion trajectories $(\hat{\theta}_h, \hat{\dot{\theta}}_h, \hat{\ddot{\theta}}_h)$ and substitute for the pilot to drive the exoskeleton through an impedance model and the torque is $\hat{\tau}_h$ provided by the impedance model. The model-based controller not only amplify the forces initiated by the interaction predictor but also the forces imposed by the pilot to correct the errors between the predictive motion trajectory and the intended motion trajectory of the pilot, the torque provided by the model-based controller is represented by τ_c. The details of the MIP strategy will be introduced this section.

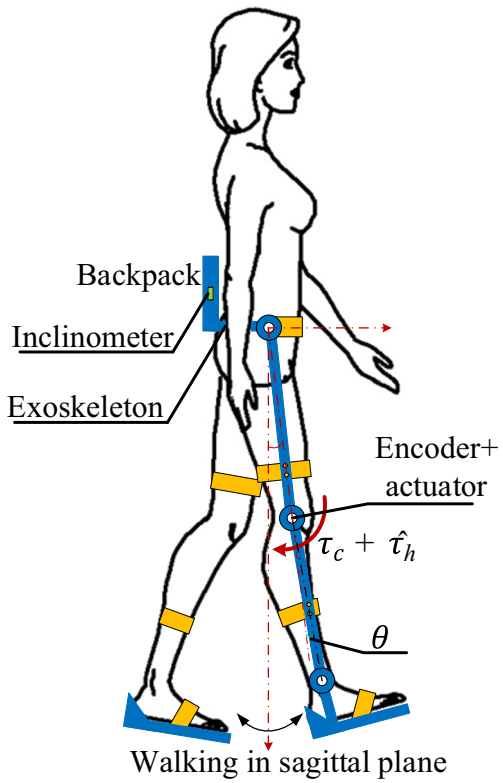

Fig. 1 An exoskeleton interacting with a pilot during walking motion

2.1 Interaction Predictor

The main purpose of the interaction predictor is to generate a proactive control strategy for assisting motions of the pilot. The interaction predictor mainly consists of a trajectory generator and an impedance model. The trajectory generator is mainly used for generating predictive motion trajectories of the pilot base on gait descriptors, the trajectories are treated as the motions performed by a virtual pilot synchronized with the real pilot. Then the impedance model maps the motion trajectories to the control strategies which are imposed on the exoskeleton. In this section, we will present how we predict motion trajectories of the pilot and how the predictive motion trajectories are mapped to control strategies.

2.1.1 Trajectory Generator of Pilot's Motion

Learning by demonstration methods have widely used in imitation learning of robots. In human-coupled robot applications, it is used to model the goal motion trajectory through human demonstrations. In which, DMP is known for the outstanding performance of imitation learning. It is used as a powerful representation tool to model human movement trajectories [2, 3, 9–11]. During the interaction between pilot and lower extremity exoskeleton, we can consider the process that the pilot changes his/her motion patterns as the demonstration process. And the trajectories demonstrated by the pilot are recorded as the trained dataset (gait descriptors) of imitation learning. For the purpose of incrementally learning motion trajectory online, DMP is updated by an incrementally learning modular with LWR. Due to the rhythmic nature of pilot's motions, the reshaped motion trajectories can be used to predict the motion trajectory of the pilot (i.e. the rhythmic nature promises the motion trajectory of the virtual pilot to be better synchronized with the real pilot.).

DMP is divided into different types for describing different movements of robot, the limit-cycle oscillator DMP describes rhythmical movements [12], while discrete movements are described by the discrete acceleration DMP. In this paper, we choose the limit-cycle oscillator DMP to model motion trajectories of the pilot. The limit-cycle

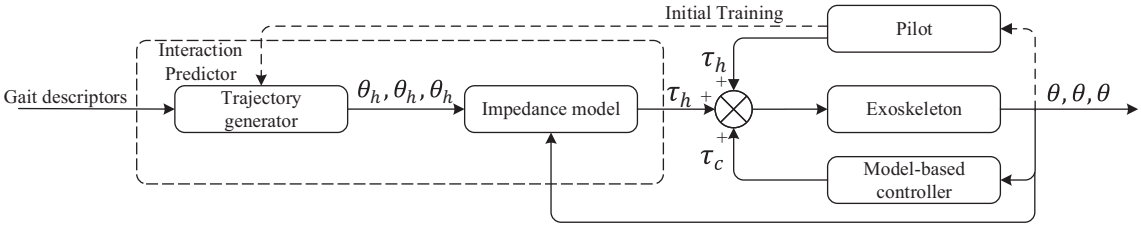

Fig. 2 Control diagram of MIP control strategy consisted of an interaction predictor and a model-based controller

oscillator DMP is defined as follows:

$$\begin{cases} \tau \dot{z} = \frac{\mu}{E_0}(E - E_0)z - k^2 u \\ \tau \dot{u} = z, where E = (z^2 + k^2 u^2)/2, \end{cases} \tag{1}$$

where μ and k are positive parameters related to the stiffness and damping of the oscillator. We can adjust τ to determine the frequency of the oscillator. The predictive motion trajectory $\hat{\theta}$ is calculated by Eq. 2:

$$\tau \dot{\hat{\theta}} = \beta(\theta_m - \hat{\theta}) + f, \tag{2}$$

where β is used as a positive constant parameter. We determine the baseline of the predictive motion trajectory $\hat{\theta}$ through adjusting θ_m. The nonlinear function f gives DMP the ability to model arbitrary trajectories. The definition of the nonlinear function is given as follows:

$$f = \frac{\sum_{i=1}^{N} \psi_i \omega_i^T \tilde{z}}{\sum_{i=1}^{N} \psi_i}, \tilde{z} = [z, \sqrt{E_0}]^T. \tag{3}$$

As shown in Eq. 3, N gaussian kernel functions are combined into the nonlinear function f. The process of motion learning is done by finding appropriate parameters ω_i of the gaussian kernel functions. The basis function of the gaussian kernels is defined as:

$$\psi_i = \exp -0.5 h_i (\phi - c_i)^2, \tag{4}$$

where the parameters h_i and c_i are the location and width of each gaussian kernel respectively. The phase variable $\phi = atan2(z, ku)$ anchors gaussian kernels. The appropriate parameters ω_i of the gaussian kernels can give us accurate models representing the motion trajectories of pilot.

We utilize LWR method to update the parameter ω_i incrementally [20] to achieve learning of the pilot's demonstration. The changing of his/her motion patterns trigger the learning process, and the motion trajectories θ_d recorded by the exoskeleton used to find the regression goal f_g. It can be calculated through Eq. 5 based on the motion trajectories θ_d.

$$f_g = \tau \dot{\theta}_d - \beta(\theta_m - \theta_d). \tag{5}$$

The detailed learning process of LWR is illustrated in Algorithm 1. The default weighted parameters ω_i derived from the learning of clinical normal walking trajectories. During operation, the time of latest gait cycle determine the frequency parameter τ, and the nonlinear function f_g is used to find optimal weighted parameters ω_i. In order to speed up the learning process, the weighted parameters ω_i are initialized with the historical DMP from last gait cycle.

Algorithm 1 Increment learning process using locally weighted regression.

1: Obtain reshaped motion trajectories from pilot's demonstration;
2: Update τ based on the time of latest gait cycle;
3: Initialize ω_i with historic DMPs of latest gait cycle;
4: Calculate f_g based on the reshaped trajectories by Eq. 5;
5: **repeat**(For N Gaussian kernels $i \in [1, N]$)
6: $\quad \omega_i \leftarrow \omega_i + P_i \tilde{z} e_i$;
7: $\quad P_i \leftarrow \frac{1}{\lambda}(P_i - \frac{P_i \tilde{z} \tilde{z}^T P_i}{\frac{\lambda}{\psi_i} + \tilde{z}^T P_i \tilde{z}})$;
8: **until** Until $e_i = |f_g - \omega_i \tilde{z}| < \varepsilon$ (ε is a small positive number)

2.1.2 Impedance Model

After obtaining the predictive motion trajectory, we will consider how the exoskeleton follows the predictive motion trajectory accurately (i.e. synchronize the movements of the exoskeleton and the pilot). In general exoskeleton systems, the interaction forces can be transferred to the exoskeleton through compliant connections and the compliant connections are modeled as impedance models [8–11]. So, we utilize impedance model as the function which can map the predictive motion trajectories of the pilot to the torques imposed on joints of the exoskeleton. The impedance model is represented as:

$$\hat{\tau}_h = k_s(\hat{\theta}_h - \theta) + k_d(\dot{\hat{\theta}}_h - \dot{\theta}), \tag{6}$$

where k_s and k_d are positive quantities, $\hat{\theta}_h$ and $\dot{\hat{\theta}}_h$ are predictive motion trajectories of the pilot (joint angle and angular velocity) generated by the trained DMP model.

2.2 Model-based Controller

In the MIP strategy, the model-based controller is utilized to amplify the forces provided by the interaction predictor.

Another more critical role is to assist the pilot correct the errors between the predictive motion trajectory and the intended motion trajectory of the pilot. By this way, even if the model-based controller uses inaccurate dynamic models, the exoskeleton can achieve better performance following the pilot's motion. In this paper, the model-based controller (i.e. the SAC algorithm) which is proven to be stable [14] is defined as:

$$\tau_c = mgl \cdot \sin\theta + (1 - \alpha^{-1})(\hat{J}\ddot{\theta} + \hat{B}\dot{\theta}). \tag{7}$$

Estimated dynamic parameters $\hat{J}$ and $\hat{B}$ of the exoskeleton (the inertial moment and viscous friction coefficient parameters) are usually obtained by identification methods and they are not accurate enough in most real-time applications. The mass and length of the exoskeleton are represented by m and l respectively. g represents the gravitational constant and α is the sensitivity factor.

3 Experiments and Discussions

In this section, we designed different experiments to explore the characteristics of the MIP strategy, and the comparisons with traditional strategies can tell us the advantages in detail. Next, we use a simulation platform and a HUALEX platform to verify the performance. The next subsections will detail the experimental setup, results and corresponding analysis of the experiments.

3.1 Experimental Flatforms

3.1.1 Single DOF Exoskeleton Platform

In order to achieve better comparisons between the MIP strategy and traditional strategies, we design a single DOF exoskeleton platform, and the schematic diagram of the single DOF exoskeleton is illustrated as Fig. 3. Imitating the physiological structure of human leg, we designed a shank and a thigh, and they are connected by a joint. It is powered by a bi-directional linear hydraulic actuator. We integrate a force sensor at the end of the hydraulic actuator for directly obtaining the joint torque. So, the inertial dynamic of the hydraulic actuator can be ignored. We set an encoder at the knee joint to provide the joint state for our algorithm. The pilot's leg can impose forces on the exoskeleton through impedance models (simulate the compliant connection). In the strategy, the torque $\hat{\tau}_h$ provided by the interaction predictor and the torque τ_c provided by the model-based controller are imposed on the joint through actuators. In Eq. 8, τ_h represents the equivalent torques which are applied on the exoskeleton leg by the pilot's leg. The dynamic of the single DOF exoskeleton based on Lagrange can be represented as:

$$J\ddot{\theta} + B\dot{\theta} + mgl \cdot \sin\theta = \hat{\tau}_h + \tau_c + \tau_h, \tag{8}$$

where the letters J, B, m and l represent the inertial moment, viscous friction coefficient, mass and length of the exoskeleton leg. Note that they are different from the estimated dynamic parameters mentioned previous section. The gravitational constant is characterized by g. The joint state vector $(\theta, \dot{\theta}, \ddot{\theta})$ indicate the angle, angular velocity and angular acceleration of the exoskeleton joint.

3.1.2 HUALEX System

The HUALEX system is a highly bionic and lightweight human-robot coupling system. A pair of wearable robotic legs can transfer the load set on the backpack to the ground. In this way, the strength and endurance of pilots can be effectively enhanced. The schematic of the HUALEX system wearing by a pilot is shown in Fig. 4a. It is constructed with links which are connected together by rotating joints. There are four active joints to drive the

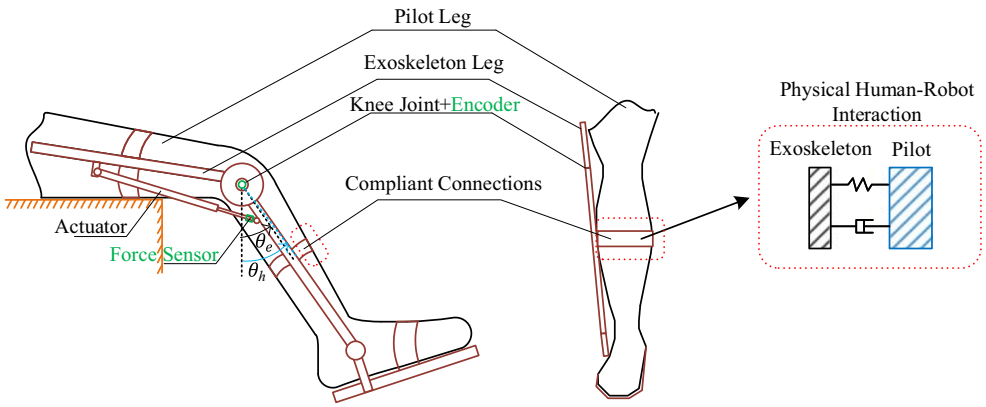

Fig. 3 The schematic diagram of the single DOF exoskeleton with the pilot's leg. The physical Human-Robot Interaction (pHRI) between the exoskeleton and the pilot is shown on the right

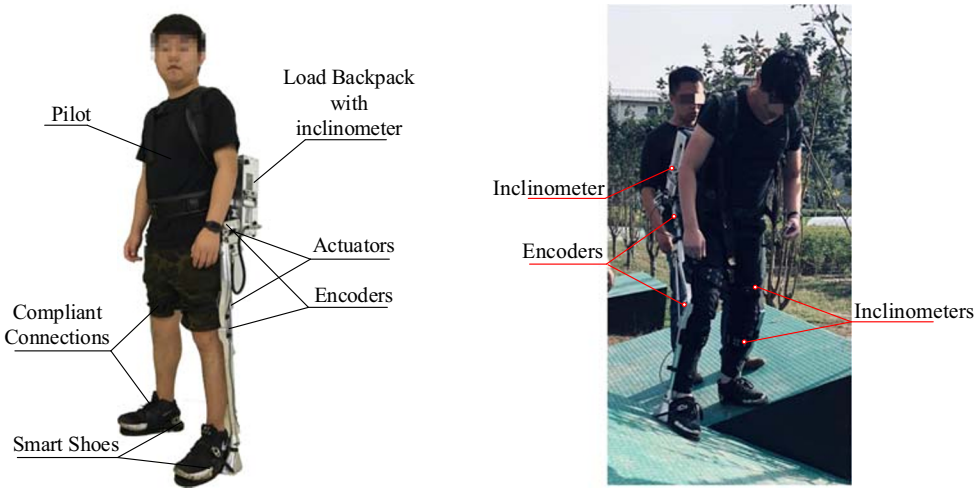

Fig. 4 **a** HUALEX is worn by a pilot. The compliant connections connect the HUALEX and the pilot into a robot-human system. The bi-directional linear hydraulic cylinders provide torques for HUALEX. The smart shoes are used for detecting the gait phases; **b** During the experiment, the joint state of the pilot was obtained by the inclinometer placed on the thigh and shank, and the encoder at the exoskeleton joint recorded the state of HUALEX

system moving, and the driving torques are derived from bi-directional linear hydraulic cylinders.

According to the study of human biomechanics and dynamics, the ankle joint mainly realizes the normal walking of the human through the energy storage mechanism [19]. Therefore, compared to the BLEEX system, energy-storage mechanism is used in the ankle joints, it can store the energy from gravity in stance phases then push the pilot forward at toe off. Simplification of the ankle joint can effectively reduce energy consumption. When a pilot wearing a HUALEX system, the pilot is attached to the HUALEX system at waist, thighs, shanks and feet.

Three kinds of sensors are used to monitor its current states. The joint angles are measured by encoders and an accelerometer set at the backpack can capture the walking velocity of the pilot. The sole pressure sensors provide the required information for judging the phase of the HUALEX. This sensor information is collected by a nearest node controller. Another function of the node controller is to control nearby actuators. The node controller can communicate with the main controller running the control algorithm via Controller Area Network (CAN).

In order to execute the MIP strategy on the HUALEX system, we first need to model the HUALEX system. The dynamic of the HUALEX system can be described as follows:

$$M(\Theta)\ddot{\Theta} + C(\Theta, \dot{\Theta}) + G(\Theta) = \hat{T}_h + T_c + T_h, \tag{9}$$

where $\Theta, \dot{\Theta}$ and $\ddot{\Theta}$ are vectors of angle, angular velocity and angular acceleration of the active joint, $\hat{T}_h$ and T_c represent the input torques from the HUALEX. The equivalent torques resulted from the pilot are represented as vector T_h. The specific functions of the torques are corresponding to Eq. 8.

The legs of lower extremity exoskeletons in different gait phases can be consider as different link mechanism as Fig. 5. Corresponding dynamic models have different parameter vectors. The swing leg can be modeled as a two-link mechanism connected to a base with a rotation joint, where the dynamic parameter matrixes $M(\Theta), C(\Theta, \dot{\Theta})$ and $G(\Theta)$ are two dimension. Unlike the swing leg, the stance leg is modeled as a three-link mechanism and the dimension are three. In which, since the structure of exoskeleton's feet has a small mass than the thigh or the shank, the ankle joint is ignored.

According to the mentioned analysis about the HUALEX system, the swing leg can be simplified as a top fixed two-link Fig. 6. The corresponding dynamic equation as follows:

$$\begin{aligned}
&M(\Theta)\ddot{\Theta} + C(\Theta, \dot{\Theta}) + G(\Theta) = \\
&\begin{bmatrix} m_2 l_1^2 + \frac{1}{3} m_1 l_1^2 + \frac{1}{3} m_2 l_2^2 + m_2 l_1 l_2 \cos\theta_2 & \frac{1}{3} m_2 l_2^2 + \frac{1}{2} m_2 l_1 l_2 \cos\theta_2 \\ \frac{1}{3} m_2 l_2^2 + \frac{1}{2} m_2 l_1 l_2 \cos\theta_2 & \frac{1}{3} m_2 l_2^2 \end{bmatrix} \begin{bmatrix} \ddot{\theta}_1 \\ \ddot{\theta}_2 \end{bmatrix} \\
&+ \begin{bmatrix} 0 & -\frac{1}{2} m_2 l_1 l_2 \sin\theta_2 \\ \frac{1}{2} m_2 l_1 l_2 \sin\theta_2 & 0 \end{bmatrix} \begin{bmatrix} \dot{\theta}_1^2 \\ \dot{\theta}_2^2 \end{bmatrix} \\
&+ \begin{bmatrix} -m_2 l_1 l_2 \sin\theta_2 & 0 \\ 0 & 0 \end{bmatrix} \begin{bmatrix} \dot{\theta}_1 \dot{\theta}_2 \\ \dot{\theta}_1 \dot{\theta}_2 \end{bmatrix} \\
&+ \begin{bmatrix} (\frac{1}{2} m_1 + m_2) g l_1 \cos\theta_1 + \frac{1}{2} m_2 g l_2 \cos(\theta_1 + \theta_2) \\ \frac{1}{2} m_2 g l_2 \cos(\theta_1 + \theta_2) \end{bmatrix} = \begin{bmatrix} \tau_1 \\ \tau_2 \end{bmatrix},
\end{aligned} \tag{10}$$

where l_1 and l_2 are the length of the shank and thigh, the corresponding mass is m_1 and m_2. θ_1 is the angle at which the link 1 deviates from the x-axis, and θ_2 is the angle at which the link 2 is offset from the link 1. τ_1 and τ_2 represent the total torque applied to the hip and knee joints,respectively. Therefore, the MIP strategy for HUALEX can be designed as:

$$T_c = G(\Theta) + (1 - \alpha^{-1})(\hat{M}(\Theta)\ddot{\Theta} + \hat{C}(\Theta, \dot{\Theta})), \tag{11}$$

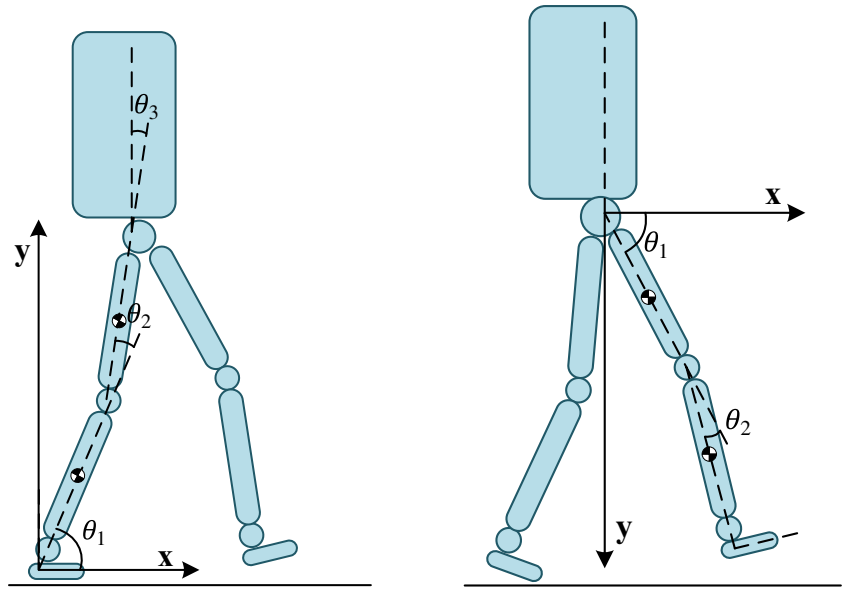

(a) Stance phase (b) Swing phase

Fig. 5 The exoskeleton leg can be modeled as a two-link mechanism connected by a rotation joint in stance phase. The corresponding swing phase, the exoskeleton leg is modeled as a three-link mechanism

$$\hat{T}_h = k_s(\hat{\Theta}_h - \Theta) + k_d(\hat{\dot{\Theta}}_h - \dot{\Theta}), \tag{12}$$

Because the thighs and shanks of the HUALEX system are not homogeneous links, the design parameters of the 3-dimensional model are used in the controllor.

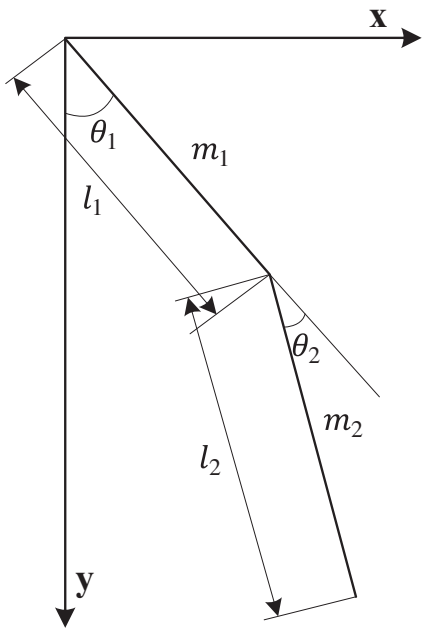

Fig. 6 The model of Top fixed two-link

3.2 Experimental Setup

3.2.1 Single DOF Exoskeleton Platform

We use open source Gazebo 7.0 simulation software to model the single DOF exoskeleton, in which the dynamic model parameters J, B, m, l, g of the shank are set as recommended physical parameters of a $0.3 \times 0.03 \times 0.03\ m^3$ rotary link. The interaction dynamic (compliant connections) is modeled as an impedance model:

$$\tau_h = k_c(\theta_h - \theta) + k_b(\dot{\theta}_h - \dot{\theta}), \tag{13}$$

where k_c and k_b are the positive stiffness and damping parameter respectively and set to 100 and 10, determined empirically. θ_h and $\dot{\theta}_h$ are the pilot's joint angle and angular velocity which are given in advance. Before the simulation experiment start, we train the DMP of the interaction predictor with a given motion trajectory. The weights initialized with offline gait datas can improve the imitation learning process in first gait cycle. During pilot's operaction, when the pilot changes his/her motion pattern, the weights can be updated incrementally based on the weights of latest gait cycle. In our experiments, the k_s, k_d of the interaction predictor and the sensitivity factor α of the model-based controller are set to 100, 10 and 100 empirically. And, we set the number of gaussian kernels to 25 and the incrementally learning process will be terminated when the terminal condition $\varepsilon = 0.5$ is met.

In this section, we carry out two experiments on the simulation platform, the first experiment is used to simulate the normal walking pattern of pilots. In which, we use periodic sine waves to represent pilot's rhythmic movement. The angular frequency of the sine waves is set as $2\pi/s$ and the amplitude is $\pi/6$. Second experiment, the input of the pilot's motion trajectories is replaced by periodic sine waves with different frequencies and amplitudes. Different frequencies and amplitudes are used to simulate different pilots and walking patterns. In this experiment, totally 9 cycles swing movement trajectories (the angular frequencies are approximately set with $2\pi/s$ and $4\pi/s$, and the amplitudes are approximately set as $\pi/6$ and $\pi/4$) are employed as the predefined pilot trajectories.

3.2.2 HUALEX System

In the experiments on the HUALEX system, we randomly choose three pilots (A, B, C) with different heights (168cm, 174cm, 182cm) from our lab to operate the HUALEX system independently with varying walking speed from 0.4m/s to 1.2m/s. Among them, the operation experience has been experienced. So, there are not training sessions for the pilots. The parameters of the MIP strategy are set to same values as the simulation experiment. Before starting the experiments, the DMP model is trained initially through normal walking motion trajectories obtained from gait capture system (VICON). During the operating, the plantar sensor can tell the MIP strategy the start and end time of each gait cycle, and the accelerometer set at the backpack measures the walking speed of the pilot which relate to the frequency parameters of the DMP model. In order to show the performance of the proposed MIP strategy in practical application, we additionally set four inclinometers on the thighs and shanks of the pilot to get the states of the pilot as Fig. 4a.

3.3 Experimental Results

3.3.1 Single DOF Exoskeleton Platform

The first simulation experiment is to compare the proposed MIP with traditional SAC algorithm, in which the accurate dynamic models determined by the design are employed. During the experiment, the interaction forces calculated by Eq. 13, the pilot's joint angles given in advance and the exoskeleton's joint angles read directly from the API interface provided by the simulation software are used to show the performance of the strategies in Figs. 7 and 8. Fig. 7 depicts the comparison of the MIP strategy and the SAC algorithm with rhythmic patterns. We can intuitively from the figures that there is a significant reduction in interaction forces compared to traditional SAC algorithm.

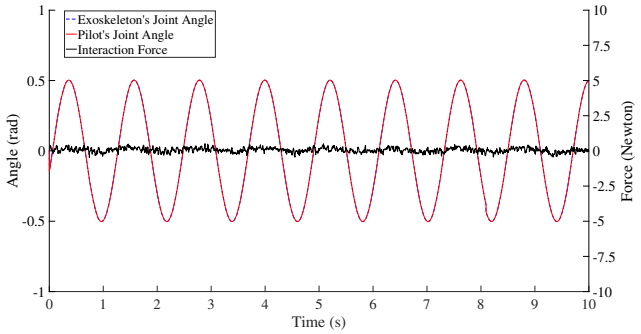

(a) MIP algorithm

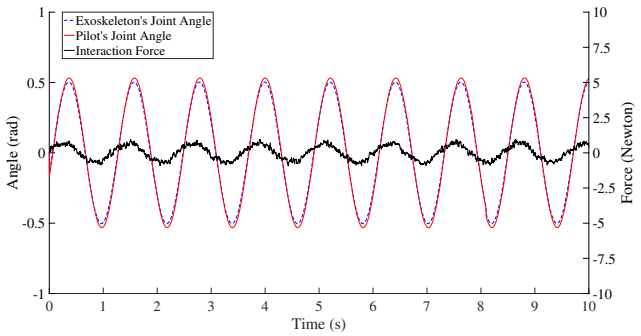

(b) SAC algorithm

Fig. 7 Comparison of control performances with accurate dynamic models of **a** MIP strategy: nMSE(MIP) = 0.002 rad; **b** SAC strategy: nMSE(SAC) = 0.015 rad

We attribute this significant reduction to the addition of the interaction predictor.

The SAC algorithm to follow the motion of the pilot through amplificate the interaction forces imposed by the pilot. In other words, the interaction force must exist although the accurate dynamic models is exist. However the interaction predictor replace the pilot to drive the exoskeleton in the MIP strategy, so the interaction forces between the exoskeleton and the pilot can be little. And in the top figure, the joint trajectories of the pilot and the exoskeleton are too close to make they almost indistinguishable. The part of the perfect following performance is contributed by the perfect period pilot's motion which make it easier for the trajectory generator to estimate the pilot's motion.

In order to show the possibility of our strategy responding to different walking patterns. we use the sine waves with different frequencies and different amplitudes for simulating different walking patterns of human in real life. The sine waves are not a simple combination of different frequency and different amplitude waves, we did some optimizations at the connection points. By this way, the sine waves have a smooth transition which can avoid larger interaction forces resulted from a unnatural transition and is more in line with realistic walking patterns. As

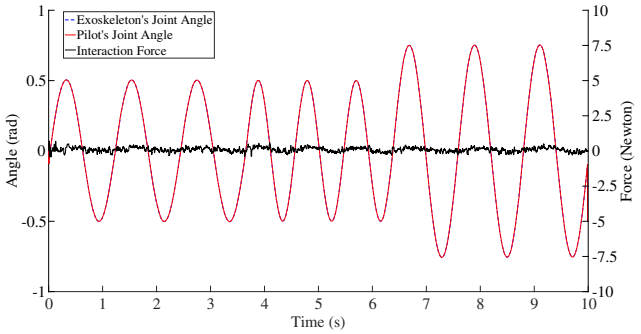

(a) MIP algorithm

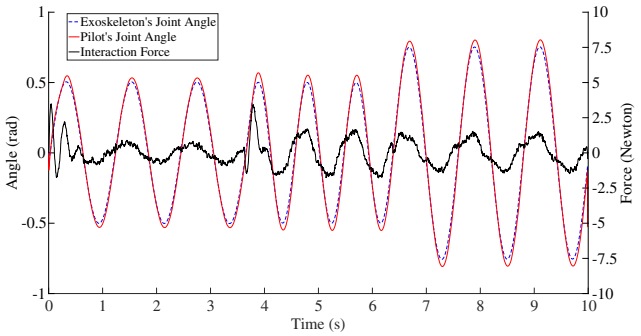

(b) SAC algorithm

Fig. 8 Comparison of control performances with accurate dynamic models of (a) MIP strategy: nMSE(MIP) = 0.005 rad; (b) SAC strategy: nMSE(SAC) = 0.045 rad

shown in Fig. 8, the proposed MIP strategy demonstrates its superiority through that the MIP strategy have smaller interaction forces, the SAC algorithm does not. But, the interaction forces of the proposed MIP strategy has a increase when the motion pattern of the pilot changes, since the pilot need move the exoskeleton forcibly to correct the errors between the predictive motion trajectory and the intended motion trajectory (such as in the first gait cycle and the switching point of different walking patterns). After obtaining the reshaped motion trajectories, the interaction force of the proposed MIP can return to small. Compared with the traditional SAC algorithm, the increase is negligible because most of the interaction forces is borne by the interaction predictor. And, we calculate the normalized Mean Square Error (nMSE) tracking angle trajectories of the pilot, they can convince us that the MIP strategy have batter performances in lower extremity exoskeleton (0.005 rad compare with 0.045 rad). Of course, the perfect periodic pilot's motion and the small changes in amplitude and frequency contribute to the perfect performance of the MIP strategy.

SAC algorithm is a typical model-based control algorithm. The fundamental problem also exists in it, which is that dynamic model parameters of the system (exoskeleton in this paper) must be accurate enough. In order to prove the key advantage that the proposed MIP strategy can lower dependency on the accurate dynamic model of exoskeletons, we design another experiment to verify that the MIP strategy can effective lower dependency on the accurate dynamic model of exoskeletons.

In this experiment, we set two errors of the dynamic model which are set as 10% and 20% respectively (e.g. the error is 20% means that the estimated parameters $\hat{J}$ and $\hat{B}$ are chosen as $\hat{J} = 0.8J$ and $\hat{B} = 0.8B$). In Fig. 9, the interaction forces (black curves) show the response of the MIP strategy to the errors. We can see from the figure that the interaction forces do not increase significantly with the increase of the errors, and the interaction forces remain small refer to the previous performance of the traditional SAC algorithm. Similar to the previous experiments, the exitance of the interaction predictor contributes to the desire performance. In addition, we list the nMSE to show the quantitative comparison of the MIP strategy and SAC algorithm in the present of inaccurate dynamic models. From the Table 1, we can intuitively get the conclusion that the proposed MIP can effectively lower dependency on the accurate dynamic model of exoskeletons.

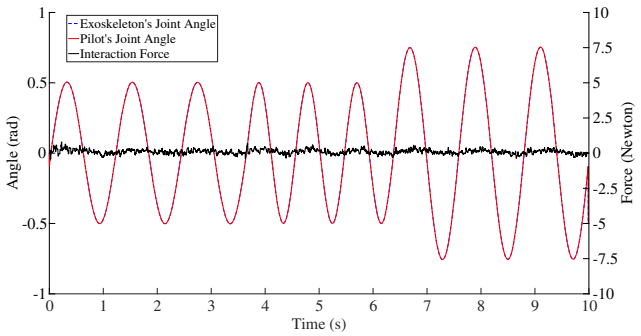

(a) MIP algorithm with 10% model error

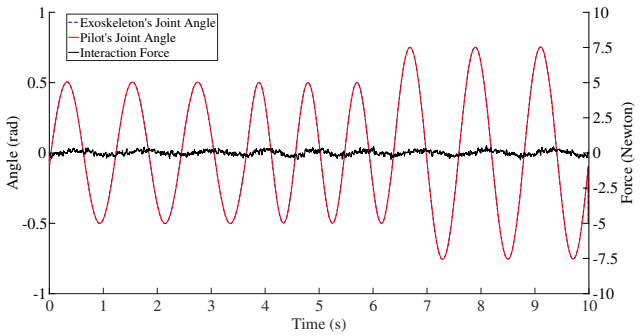

(b) MIP algorithm with 20% model error

Fig. 9 Comparison of control performances with inaccurate dynamic models of **a** MIP strategy with 10% model error: nMSE(MIP) = 0.013 rad; **b** MIP strategy with 20% model error: nMSE(MIP) = 0.032 rad

Table 1 Compensation of MIP and SAC on single DOF exoskeleton

nMSE (rad)	10% model error	20% model error	Different angular frequency
MIP	0.013	0.032	0.005
SAC	0.114	0.295	0.045

3.3.2 HUALEX System

We choose a period of whole experiment of pilot C as a representation for discussion. Figure 10a show the joint trajectories of the pilot and the exoskeleton with the proposed MIP control strategy. The proposed MIP strategy can make the exoskeleton system follow the pilot's motion with little tracking errors. Compared with the simulation experiments, we can see that there is significant mismatch at the peak and valley of the curves. After analysis, the mismatches may be caused by the defects of the mechanical structure (such as the compliant connections and the invalid stroke of the hydraulic cylinders allow a certain relative movement between the pilot's leg and the exoskeleton's leg). In addition, Fig. 10 shows the comparison of MIP with SAC algorithm at the knee joint of one pilot. It can be seen from the figure that at a position where the joint angle changes frequently, the tracking performance of MIP is significantly better than SAC. We used a spring model to calculate the interaction force between the exoskeleton and the pilot for comparisons of the tracking performance. It can be seen from the black curve in the figure that the interaction force of MIP is significantly smaller than SAC. Note that the two joint curves in Fig. 10 are slightly different because the one pilot cannot test both algorithms at the same time.

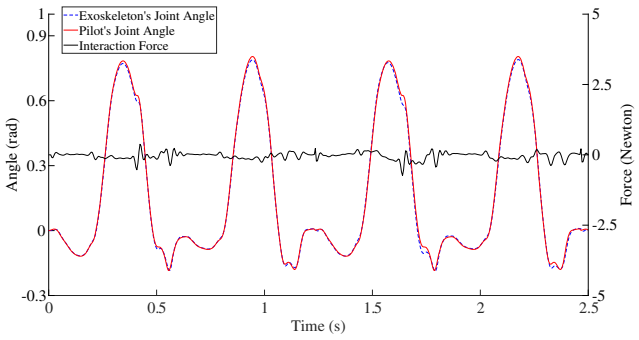

(a) MIP algorithm

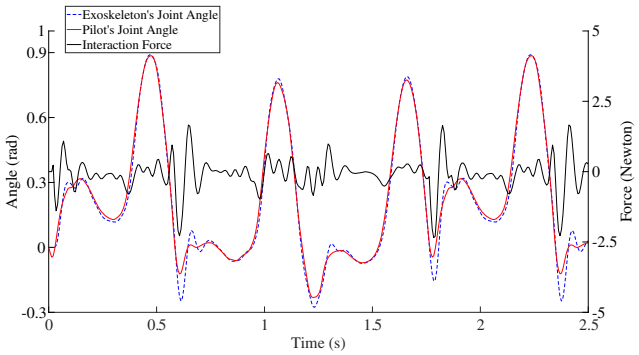

(b) SAC algorithm

Fig. 10 Control performances of the knee joint on HUALEX: **a** MIP strategy; **b** SAC strategy

Table 2 Comparison of MIP and SAC Strategy in HUALEX

nMSE(rad) (MIP|SAC)	0.4 (m/s)		0.8 (m/s)		1.2 (m/s)	
Pilot A	0.008	0.033	0.013	0.049	0.026	0.088
Pilot B	0.009	0.027	0.014	0.042	0.030	0.080
Pilot C	0.010	0.027	0.018	0.061	0.027	0.078

Table 2 shows the quantitative comparison results at left knee joint. An increase trend can be found in the table, we can also find that the increase trend of the MIP strategy is slower than the SAC algorithm. Additionally, Fig. 11 also proves the conclusions obtained from Table 2 in nMSE. So, we can conclude that the tracking performance of the MIP strategy is better than SAC algorithm.

4 Conclusions and Future Works

This paper has proposed a novel MIP strategy, which aims to lower dependency on the accurate dynamic model of exoskeletons. In the MIP strategy, the interaction predictor can predict motion trajectories of the pilot and substitute for the pilot to drive the exoskeleton through an impedance model. The model-based controller not only amplify the forces initiated by the interaction predictor, but more importantly the forces imposed by the pilot to correct the errors between the predictive motion trajectory and the intended motion trajectory.

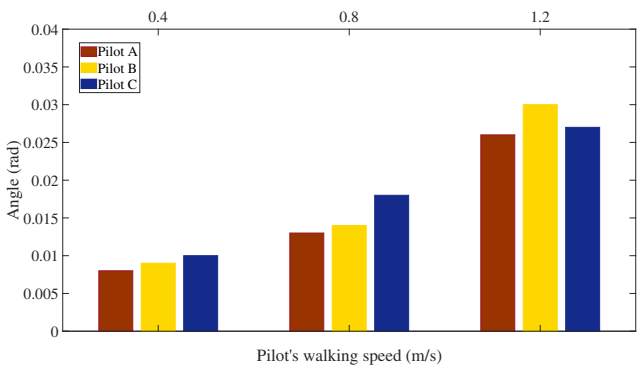

Fig. 11 The nMSE of the joint trajectories between HUALEX and pilot with different walking speeds

In this paper, we determine the weights of the interaction predictor and the moedel-based controller based on our experience. In the future, we will investigate in the coupling relationship of the weights between the interaction predictor and the model-based controller. How does the weights affect the dependency on accurate dynamic models. How to determine the weights according to the desire the dependency.

Acknowledgements This work was made possible by support from the National Key Research and Development Program of China (No. 2017YFB1302300), National Natural Science Foundation of China (NSFC) (No. 6150020696, 61503060), Sichuan Science and Technology Major Projects of New Generation Artificial Intelligence (No. 2018GZDZX0037) and the Fundamental Research Funds for the Central Universities (No. ZYGX2015J148).

References

1. Calzado, J., Lindsay, A., Chen, C., Samuels, G., Olszewska, J.: SAMI: Interactive, multi-sense robot architecture. In: IEEE 22nd International Conference on Intelligent Engineering Systems (INES), pp. 317–322 (2018)
2. Chen, Q., Cheng, H., Yue, C., Huang, R., Guo, H.: Step length adaptation for walking assistance. In: IEEE International Conference on Mechatronics and Automation (ICMA), pp. 644–650 (2017)
3. Chen, Q., Cheng, H., Yue, C., Huang, R., Guo, H.: Dynamic balance gait for walking assistance exoskeleton. Applied Bionics and Biomechanics, pp. 1–10 (2018)
4. Ding, Y., Galiana, I., Siviy, C., Panizzolo, F.A., Walsh, C.: IMU-based iterative control for hip extension assistance with a soft exosuit. In: IEEE International Conference on Robotics and Automation (ICRA), pp. 3501–3508 (2016)
5. Ghan, J., Kazerooni, H.: System identification for the Berkeley Lower Extremity Exoskeleton (BLEEX). In: IEEE International Conference on Robotics and Automation (ICRA), pp. 3477–3484 (2006)
6. Ghan, J., Steger, R., Kazerooni, H.: Control and system identification for the Berkeley Lower Extremity Exoskeleton (BLEEX). Adv. Robot. **20**(9), 989–1014 (2006)
7. Huang, L., Steger, R.R., Kazerooni, H.: Hybrid control of the Berkeley Lower Extremity Exoskeleton (BLEEX). In: International Mechanical Engineering Congress and Exposition, pp. 1429–1436 (2005)
8. Huang, R., Cheng, H., Chen, Q., Tran, H.T., Lin, X.: Interactive learning for sensitivity factors of a human-powered augmentation lower wxoskeleton. In: IEEE International Conference on Intelligent Robots and Systems (IROS), pp. 6409–6415 (2015)
9. Huang, R., Cheng, H., Guo, H., Chen, Q., Lin, X.: Hierarchical interactive learning for a human-powered augmentation lower exoskeleton. In: IEEE International Conference on Robotics and Automation (ICRA), pp. 257–263 (2016)
10. Huang, R., Cheng, H., Guo, H., Lin, X., Chen, Q., Sun, F.: Learning cooperative primitives with physical human-robot interaction for a HUman-Powered Lower EXoskeleton. In: IEEE International Conference on Intelligent Robots and Systems (IROS), pp. 5355–5360 (2016)
11. Huang, R., Cheng, H., Guo, H., Lin, X., Zhang, J.: Hierarchical learning control with physical human-exoskeleton interaction. Inform. Sci. **432**, 584–595 (2018)
12. Ijspeert, A.J., Nakanishi, J., Schaal, S.: Learning rhythmic movements by demonstration using nonlinear oscillators. In: IEEE International Conference on Intelligent Robots and Systems (IROS), vol. 3, pp. 958–963 (2002)
13. Kazerooni, H., Chu, A., Steger, R.: That which does not stabilize, will only make us stronger. Int. J Robotics Res. **26**(1), 75–89 (2007)
14. Kazerooni, H., Racine, J.L., Huang, L., Steger, R.: On the control of the Berkeley Lower Extremity Exoskeleton (BLEEX). In: IEEE International Conference on Robotics and Automation (ICRA), pp. 4353–4360 (2005)
15. Kazerooni, H., Steger, R.: The Berkeley Lower Extremity Exoskeleton. Journal of Dynamic Systems, Measurement and Control **128**(1), 14–25 (2006)
16. Li, Z., Ma, W., Yin, Z., Guo, H.: Tracking control of time-varying knee exoskeleton disturbed by interaction torque. ISA Trans. **71**, 458–466 (2017)
17. Ng, A.Y., Coates, A., Diel, M., Ganapathi, V., Schulte, J., Tse, B., Berger, E., Liang, E.: Autonomous inverted helicopter flight via reinforcement learning. In: Experimental Robotics IX, pp. 363–372. Springer (2006)
18. Nguyen-Tuong, D., Peters, J.R., Seeger, M.: Local Gaussian process regression for real time online model learning. In: Advances in Neural Information Processing Systems, pp. 1193–1200 (2009)
19. Olszewska, J.I., Houghtaling, M., Goncalves, P.J., Fabiano, N., Haidegger, T., Carbonera, J.L., Patterson, W.R., Ragavan, S.V., Fiorini, S.R., Prestes, E.: Robotic standard development life cycle in action. Journal of Intelligent & Robotic Systems, pp. 1–13 (2019)
20. Schaal, S., Atkeson, C.G.: Constructive incremental learning from only local information. Neural Comput. **10**(8), 2047–2084 (1998)
21. Steger, R., Kim, S.H., Kazerooni, H.: Control scheme and networked control architecture for the Berkeley Lower Extremity Exoskeleton (BLEEX). In: IEEE International Conference on Robotics and Automation (ICRA), pp. 3469–3476 (2006)
22. Tran, H.T., Cheng, H., Lin, X., Duong, M.K., Huang, R.: The relationship between physical human-exoskeleton interaction and dynamic factors: using a learning approach for control applications. Science China Information Sciences **57**(12), 1–13 (2014)
23. Tutsoy, O.: CPG based RL algorithm learns to control of a humanoid robot leg. Int. J. Robot. Autom. **30**(2), 1–7 (2015)
24. Walsh, C.J., Paluska, D., Pasch, K., Grand, W., Valiente, A., Herr, H.: Development of a lightweight, underactuated exoskeleton for load-carrying augmentation. In: IEEE International Conference on Robotics and Automation (ICRA), pp. 3485–3491 (2006)
25. Wang, Y., Gao, F., Doyle, F.J. III.: Survey on iterative learning control, repetitive control, and run-to-run control. J. Process. Control. **19**(10), 1589–1600 (2009)
26. Winter, D.A.: Biomechanics and Motor Control of Human Movement. Wiley, Hoboken (2009)

Guangkui Song is a Ph.D. student at the Center for Robotics, School of Automation and Engineering, University of Electronic Science and Technology of China. His research interest include applied robotics, mainly in the fields of robot control, human-robot interaction, adaptive control and imitation learning.

Rui Huang (M'18) received the Ph.D. degree in control science and engineering from the University of Electronic Science and Technology of China (UESTC), Chengdu, China, in July 2018. He was a joint training doctoral student with TAMS, University of Hamburg, Hamburg, Germany, from 2016 to 2017. He is a post-doctor at the Center for Robotics, School of Automation Engineering, UESTC. His current research interests include reinforcement learning, rehabilitation robot, human-robot interaction, and robot control.

Jing Qiu received the Ph.D. degree in human factors and ergonomics from the Darmstadt University of Technology, Darmstadt, Germany, in 2010. She is currently an Associate Professor with the Center for Robotics, School of Mechanical Engineering, University of Electronic Science and Technology of China, Chengdu, China. Her current research interests include human factors in exoskeleton, human-robot interaction, and rehabilitation robot.

Hong Cheng (M'06-SM'14) received the Ph.D. degree in pattern recognition and intelligent systems from Xi'an Jiaotong University (XJTU), Xi'an, China, in 2003. He is currently a Full Professor with the School of Automation and the Vice Director of the Center for Robotics, University of Electronic Science and Technology of China, Chengdu, China, (UESTC), where he is currently the Founding Director of the Machine Intelligence Institute. Before this, he held a post-doctoral position at the Computer Science School, Carnegie Mellon University, Pittsburgh, PA, USA, from 2006 to 2009. He has been an Associate Professor with XJTU since 2005. Since 2000, he has been with XJTU, where he has been a Team Leader of the Intelligent Vehicle Group, Institute of Artificial Intelligence and Robotics, before going to the USA. The team that he was leading in XJTU developed an intelligent driving platform-Spring robot, which has an important social effect in China. His current research interests include computer vision and machine learning, robotics, human-computer interaction, and multimedia signal processing. Dr. Cheng is a Senior Member of the ACM. He is a reviewer of many important journals and conferences (IEEE TITS, MAV, CVPR, ICCV, ITSC, IVS, and ACCV). He serves as the Registration Chair for 2005 IEEE ICVES, the Local Arrangement Chair for VLPR 2012, and the Finance Chair for ICME 2014. He is also an Associate Editor of the IEEE Computational Intelligence Magazine.

Shuai Fan is a Ph.D. student at the School of Mechanical and Electrical Engineering, University of Electronic Science and Technology of China. His main field of research is applied robotics which specifically includes multi-duty parallel manipulators, defect identification and dynamic analysis.